euspen's 22nd International Conference & Exhibition, Geneva, CH, May/June 2022
www.euspen.eu

# Experimental study of the effect of plectrum parameters on the performances of plucked piezoelectric energy harvesters

Ela Marković,[1] Saša Zelenika,[1, 2, 3] Petar Gljušćić [1, 2] and Marko Perčić [1, 2, 3]

[1] *University of Rijeka, Faculty of Engineering, Precision Engineering Laboratory, Vukovarska 58, 51000 Rijeka, CROATIA*
[2] *University of Rijeka, Centre for Micro- and Nanosciences and Technologies, Radmile Matejčić 2, 51000 Rijeka, CROATIA*
[3] *University of Rijeka, Centre for Artificial Intelligence and Cybersecurity, Laboratory for AI in Mechatronics, Radmile Matejčić 2, 51000 Rijeka, CROATIA*

szelenika@uniri.hr

**Abstract**
Autonomous sensor nodes, enabled by the integration of energy harvesting principles, create the preconditions for a significant simplification and mass reduction in aircraft structural health monitoring. A promising energy harvesting approach to collect and convert the energy from random aircraft vibrations during operation, is to use piezoelectric energy harvesters. Due to the narrow operating frequency bandwidth of the considered harvesters, a frequency up-conversion mechanism, based on plucking the free end of the piezoelectric devices by using rotating plectra, and letting the transducers oscillate at their eigenfrequencies, is introduced in order to enable their utilization while operating in the considered random excitation environment. An experimental investigation of fused deposition modelling 3D printed plectra is therefore carried on to better understand the effects of the respective design parameters, i.e., their size, stiffness and material types, on the resulting performances of the piezoelectric energy harvesters in terms of the obtainable specific power outputs. The voltages generated by the harvesters, as well as their maximal free end deflections, are thus measured for different plectrum materials, different plucking frequencies and different geometries of the plectra. Design-of-experiments (DoE) methods are employed in the setup of the experiments, whereas advanced numerical algorithms are used for the analysis of the hence obtained results. A comprehensive insight into the effects of plectrum properties on the responses of the piezoelectric energy harvesters is therefore provided, which represents another step towards the design of autonomous energy harvester powered sensor nodes to be used in aircraft structural health monitoring applications.

Piezoelectric energy harvesting, frequency up-conversion, autonomous sensor nodes, DoE, experimental assessment, aircraft structural health monitoring

## 1. Introduction

Structural health monitoring (SHM) of aircraft components by using non-destructive testing (NDT) techniques, is typically carried out during shutdowns or maintenance procedures, when the utilized sensors are temporarily attached to the structure [1-2]. On-board, in-process sensor nodes provide, in turn, means for real time monitoring, where SHM devices employ permanently attached sensors, signal acquisition and transfer devices, data storage and processing modules as well as automated diagnostic components [3]. The most promising approaches in aerospace SHM, including global and local monitoring as well as impact detection, employ then wave propagation, impedance and resistance technologies, optical fibres along with eddy current-based technologies, coating and vacuum monitoring systems [1, 3-4].

A thorough analysis of the airplane SHM state-of-the-art, presented in [1], clearly shows that low power requirements of the used components is one of the basic enabling factors for the development of autonomous SHM sensor nodes, comprising data elaboration and wireless communication systems. Such systems can then be integrated with devices based on energy harvesting (EH) technologies, allowing the SHM nodes to be powered by the low-level energy present in their surrounding environment (Fig. 1) [1, 3, 5-6]. This represents an important subject of the research work performed in the framework of the EU COST Action CA18203 "Optimising Design for Inspection" (ODIN) [7].

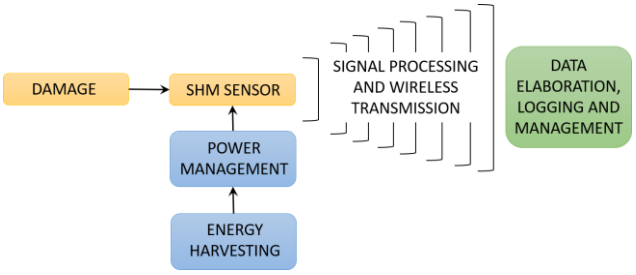


**Figure 1.** Schematic representation of an autonomous SHM node [1].

Of the energy forms available on and around an operating aircraft, i.e., solar, kinetic, thermal, acoustic, and radio frequency energy sources, kinetic energy is seen as one of the most viable options [1, 5-6]. Due to its simplicity, reliability, scalability and relatively high conversion efficiency, the most common EH mechanism aimed at collecting and converting kinetic into electrical energy, is the piezoelectric energy harvester (PEH) based on a bimorph cantilever [8-9]. A typical bimorph PEH consists of a metallic substrate between two piezoelectric layers, fixed on one end, and excited via oscillations of the clamping base (Fig. 2). The charge generated within the piezoelectric layers is collected via electrodes deposited on the piezoelectric and connected to an electrical load.

Such a device displays, however, a significant drawback, which is particularly notable under random excitation. It has, in fact, a very narrow optimal operating frequency bandwidth around its

eigenfrequency [1, 8-9]. In order to overcome this issue, and thus broaden the PEH operative range, several approaches are suggested and studied in recent literature, comprising active tuning, optimized, nonlinear and multimodal geometries and frequency up-conversion (FUC) approaches [8, 10].

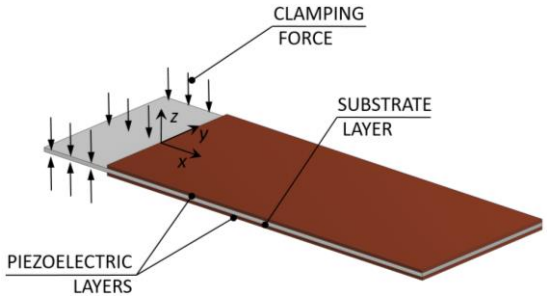


**Figure 2.** Typical bimorph PEH [11].

The FUC mechanism, addressed in this work, converts random ambient vibrations and/or strikes into a periodical excitation of the PEH free end by impacting or plucking it with a moving plectrum. The thus excited PEH is then allowed to freely oscillate at its eigenfrequency, thus maintaining the optimal operational conditions and, therefore, attaining the optimal conversion efficiency [12-14].

The parameters of the plucking process, as well as the mechanical properties, the size, the stiffness and the materials used to produce the plectra, have a strong influence on the responses of the thus excited PEH [15-16]. The understanding of these effects can be of particular significance especially when the plectra are produced by employing the cost effective and readily available 3D printing technologies, due to the specific issues innate to this technological process. In order to broaden the understanding of the effects of these influencing parameters on PEHs' responses, a thorough experimental study focused on fused deposition modelling (FDM) 3D printed plectra, is, therefore, carried on in this work.

## 2. Plectrum geometry and DoE

In order to study the effects of the geometrical and material parameters of the 3D printed plectra, several shapes of varying dimensions are initially investigated. Rectangular, elliptical and triangular shapes, as displayed in Fig. 3a, produced as segments of a six-plectra rotor (Fig. 3b), are hence considered. Due to the limitations of the manufacturing process when small-size objects are produced, the thickness of all the studied plectra is kept constant at $t$ = 0.7 mm. Since the variation of the plectrum dimensions mostly affects their stiffness, the range of dimensions is thus set in such a way that a continuous and uniform stiffness range can be studied.

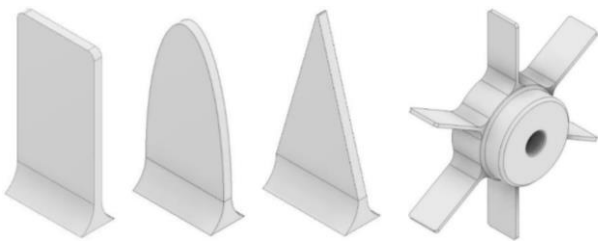

(a) (b)

**Figure 3.** Different shapes of the studied plectra (a) and the six-plectra rotor (b) [17].

Based on the initially performed experiments, certain restrictions are then introduced, and a design-of-experiments (DoE) methodology [18] is employed as basis of the performed experimental measurements.

### *2.1. Experimental setup*

The experimental setup utilized in this work to provide the plucking excitation of the PEHs, comprises, as shown in Fig. 4, a DC electric motor (denoted in the Figure with 1), to which the aforementioned rotor (2) is attached. On the other hand, a rectangular PEH (3) is independently clamped to a 3D printed base (4). The value of the PEH free end displacement is then measured by using a Metrolaser® Vibromet 500V laser doppler vibrometer, while the voltage generated by the plucked PEH is measured via an Agilent® DSO-X 2012A oscilloscope [19]. In order to calculate the power generated by the PEH, the harvester is connected to the oscilloscope via a variable resistance box. The rotational speed of the DC motor is, in turn, regulated by using a controllable laboratory voltage supply.

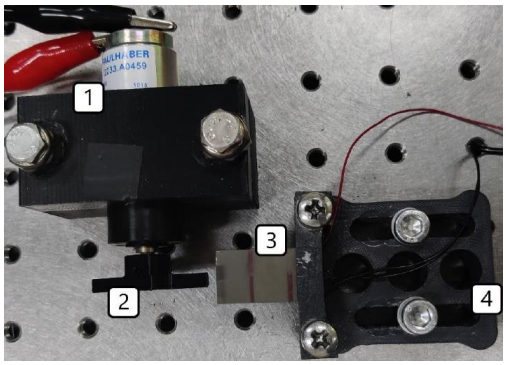


**Figure 4.** Experimental setup for generating plucking excitations [17].

### *2.2. Initial studies*

Initial studies consisted in using the different plectrum shapes and sizes to excite the rectangular PEH, thus obtaining a voltage and power response. Due to aforementioned limitations of the 3D printing process, the actual geometry of the elliptical and triangular plectra differed, however, significantly from the 3D model, which, in turn, significantly affected the actual stiffness of the respective plectra. All of this caused noteworthy repeatability issues noticed in the PEH response results.

With this in mind, it was established that the rectangular shape most accurately corresponded to the respective 3D model (Fig. 5a) and it was, therefore, selected for further studies. Due to the fact that objects printed as segments of the six-plectra rotor in different positions, i.e., at different printing angles, possess different mechanical properties [20-21], the overall shape of the rotor is also changed to a symmetrical two-plectra design (Fig. 5b), which ultimately lead to a substantial improvement of the overall measurement repeatability.

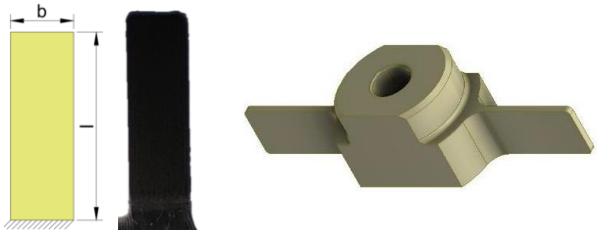


(a) (b)

**Figure 5.** Illustration of the rectangular plectrum with the respective 3D printed version (a) and the symmetrical two-plectra rotor (b) [17].

### *2.3. Design-of-experiments*

In order to reduce the number of required experimental measurements, while maintaining the accuracy of the attained

results, 20 combinations of variable parameters are generated using the Latinized Centroidal Voronoi Tessellation (LCVT) DoE methodology [18]. For that purpose, four separate variable parameters are selected:

- three variables defining the plectrum properties, i.e., the plectrum material, the area moment of inertia $I_x$ and the length of the plectrum $l$, and
- one parameter influencing the plucking conditions, namely the rotating speed $n_0$ of the DC motor.

The herein considered plectrum materials, defined as a discrete variable, are polyamide (PA), polycarbonate (PC), acrylonitrile butadiene styrene (ABS) and polylactic acid (PLA). Albeit having all comparable mechanical properties [17], these materials vary in terms of the respective surface roughness characteristics, caused by their different behaviour as an FDM 3D printing filament, which could have an influence on the PEH response as well. On the other hand, the value ranges of the studied continuous variables are listed in Table 1.

**Table 1** Value ranges of the studied variable process parameters [17].

| Process parameter | |
|---|---|
| $I_x$, mm$^4$ | 0.25 - 0.5 |
| $l$, mm | 9 - 13 |
| $n_0$, min$^{-1}$ | 60 - 200 |

## 3. Results and discussion

For the 20 process parameter combinations, generated by using the LCVT DoE methodology, the resulting 3D printed two-plectra rotors are produced by employing the FlashForge® Creator 3 3D printer [17, 22]. They are then used to excite the PEH at the corresponding rotating speeds using the described experimental setup. The thus generated RMS voltage in an oscillation cycle, subsequently averaged over 5 excitation cycles, and obtained at the previously determined PEH's optimal load resistance of 5 kΩ [11], is finally utilized to calculate the attained power outputs for each parameters' set. The average power values for all the LCVT-based DoE experimental design points are reported in Table 2.

**Table 2** Average power outputs for the DoE combinations of process parameters.

| Exp. # | Material | $P$, mW | Exp. # | Material | $P$, mW |
|---|---|---|---|---|---|
| 1 | PC | 1.180 | 11 | ABS | 0.237 |
| 2 | ABS | 0.713 | 12 | PA | 0.308 |
| 3 | PA | 0.613 | 13 | PC | 0.482 |
| 4 | ABS | 0.789 | 14 | PC | 0.838 |
| 5 | ABS | 0.268 | 15 | ABS | 0.243 |
| 6 | PA | 0.827 | 16 | PLA | 0.155 |
| 7 | PLA | 0.764 | 17 | PC | 0.833 |
| 8 | PC | 0.631 | 18 | PA | 0.510 |
| 9 | PA | 0.268 | 19 | PLA | 0.662 |
| 10 | PLA | 0.823 | 20 | PLA | 0.313 |

The experimentally obtained power outputs range, thus, from $P \approx 0.16$ mW, for a 12.2 mm long PLA plectrum with $I_x = 0.25$ mm$^4$ rotating at $n_0 = 144.4$ min$^{-1}$, up to $P \approx 1.18$ mW for a 9 mm long PC plectrum with $I_x = 0.333$ mm$^4$ rotating at $n_0 = 132.8$ min$^{-1}$.

The thus acquired data is analysed using the response surface methodology, resulting in a quadratic regression equation (1) with three variables [23-24], while the respective constants for each of the four material types are listed in Table 3.

$$P = a - b \cdot I_x - c \cdot n_0 - 2.04 \cdot l + 15.3 \cdot I_x^2 + \\ +4.2 \cdot 10^{-5} \cdot n_0^2 + 8.79 \cdot 10^{-2} \cdot l^2 + 0.1234 \cdot I_x \cdot n_0 + \\ +1.305 \cdot I_x \cdot l + 2.92 \cdot 10^{-3} \cdot n_0 \cdot l \quad (1)$$

**Table 3** Quadratic regression model constants for the four different studied plectrum materials.

| Constant | PA | PC | ABS | PLA |
|---|---|---|---|---|
| $a$ | 23.5 | 16.7 | 23.9 | 19.2 |
| $b$ | 17.1 | 2.17 | 18.8 | 8.9 |
| $c$ | 0.098 | 0.083 | 0.095 | 0.086 |

The obtained coefficient of determination [25-26] with a value of $R^2 = 99.4\%$ implies a high predictive accuracy of the used quadratic model, which, thus, describes more than 99% of the variance of the studied process parameters.

When a Generalized Reduced Gradient (GRG2) code-based optimization algorithm [27], having as a goal function the maximization of the power output, is applied to the quadratic model of Equation (1) within the process parameters' ranges listed in Table 1, it is found that a maximal power output $P_{max} \approx 5.1$ mW can be achieved with a $l = 9$ mm long PC plectrum having the area moment of inertia $I_x = 0.5$ mm$^4$ and rotating at $n_0 = 200$ min$^{-1}$. The maximal achievable power values, along with the corresponding values of the studied process parameters, for all the considered plectrum materials, are reported in Table 4.

**Table 4** Maximum power outputs and optimal parameters for different plectrum materials.

| Material | PA | PC | ABS | PLA |
|---|---|---|---|---|
| $P_{max}$, mW | 3.72 | 5.06 | 3.85 | 3.46 |
| $I_x$, mm$^4$ | 0.25 | 0.5 | 0.25 | 0.5 |
| $l$, mm | 9 | 9 | 9 | 9 |
| $n_0$, min$^{-1}$ | 60 | 200 | 60 | 200 |

Based on the data in Table 4, it can be concluded that the optimal process parameter values, resulting in the considered cases in the highest power outputs, correspond to different combinations of the upper and lower limits of the values of $I_x$ and $n_0$. In terms of the plectrum length, the model clearly converges, in turn, towards a shorter, i.e., stiffer plectrum.

Since the minimal plectrum length is found to be the optimal one for all the four considered 3D printed materials, response surface graphs can be generated, representing the power outputs achievable by using the $l = 9$ mm long plectra, as shown in Figure 6. From the depicted data it is thus clear once more that a combination of the process parameter values at the limits of the specified value ranges result in maximal power outputs. What is more, a distinct tendency to form a sort of a "saddle" is observed for all the four considered materials, suggesting that perhaps multiple maxima could occur outside of the studied value ranges of the input variable parameters. It can also be noted that the PA and ABS plectra (depicted respectively in Fig. 6a and 6c) favour a lower area moment of inertia $I_x$ as well as a lower plucking speed, while the plectra made from PC and PLA (Fig. 6b and 6d, respectively) allow obtaining the maximal power outputs at higher values of the area moment of inertia $I_x$ and at the highest considered rotational speeds.

## 5. Conclusion and outlook

With reference to the needs of on-board aircraft SHM applications based on EH-powered autonomous sensor modules, the basics of the behaviour of PEH devices is explained in this work, evidencing their characteristic drawbacks, as well as a possible solution in the form of a FUC-based plucking excitation. The effects of the respective 3D printed excitation plectra design parameters (material type, geometry and plucking conditions) on PEH's responses are then investigated on a specifically developed experimental setup. Based on the initially performed experiments, a two-rectangular-plectra rotor

is chosen, and a LCVT DoE algorithm is used to generate random combinations of selected parameters for the four different 3D printed materials affecting the plucking process. A thorough campaign of experimental measurements is thus performed.

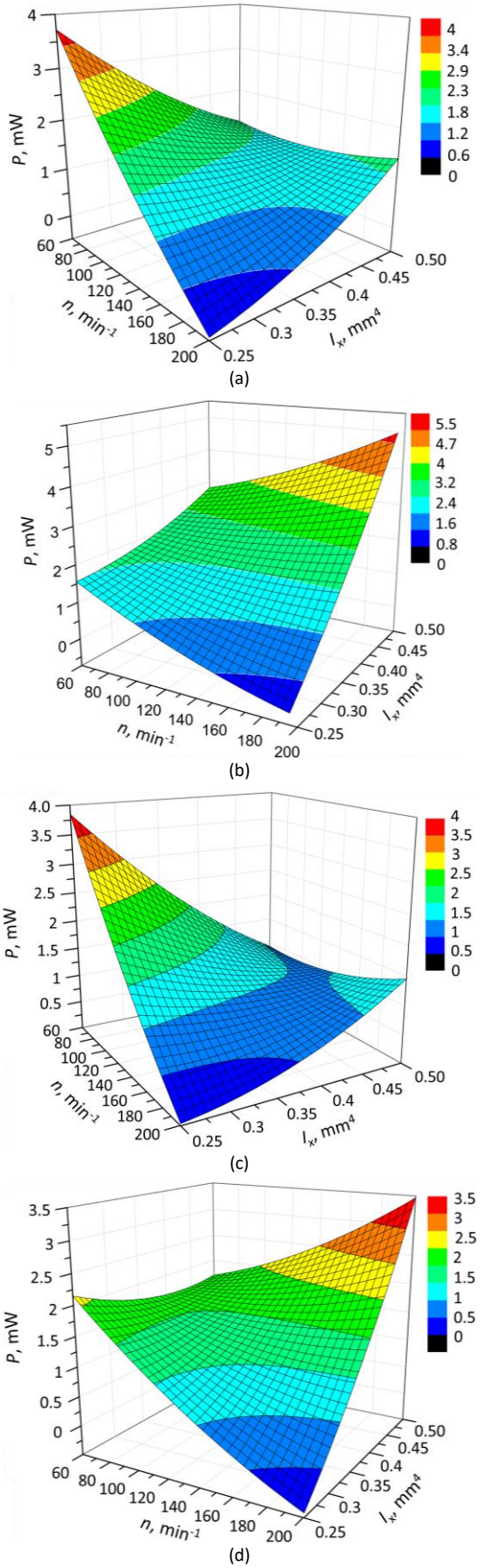


**Figure 6.** Power outputs achievable with a $l$ = 9 mm long plectrum made of PA (a), PC (b), ABS (c) and PLA (d).

The attained experimental results are utilized to develop a numerical quadratic regression model for each of the studied materials, and an excellent coefficient of determination $R^2$ = 99.4% is achieved. By applying a GRG2-based optimization algorithm to these models, the attainable power outputs are hence maximized. Based on this process it is concluded that in all the considered cases a combination of the maximal or the minimal values in the used set of process parameters value ranges results in the highest power output, and that the shortest considered plectrum length $l$ = 9 mm is optimal in all the studied cases. What is more, from the response surface graphs generated for a constant $l$ = 9 mm plectrum length, a trend to form a saddle is observed in all four models, most pronounced for the PLA plectra. This could suggest that the models might have additional maxima outside of the studied range of values of the considered process parameters, which certainly represents a direction for further studies.

The results and conclusions given in this work could form the basis for further studies of the complex plucking mechanism, and help the implementation of piezoelectric energy harvesting, as a power source, not only into in-process non-destructive SHM sensor nodes aimed for the aerospace industry, but also in other fields such as wearable devices aimed at remote patient monitoring and telemedicine, or also for IoT applications.


**Acknowledgements**

Work performed within the EU COST Action CA18203 "ODIN", enabled by using the equipment funded via the EU ERDF project RC.2.2.06-0001 "RISK", and supported by the University of Rijeka grant uniri-tehnic-18-32 "Advanced mechatronics devices for smart technological solutions".


**References**


[1] Zelenika S et al. 2020 *Sensors* **20**/22 6685
[2] Yuan F-G (ed.) 2016 *Structural Health Monitoring (SHM) in Aerospace Structures* (Sawston, UK: Woodhead Publ.)
[3] Sause M G R et al. (eds.) 2021 *Structural Health Monitoring Damage Detection Systems for Aerospace* (Cham, CH: Springer)
[4] Abbas S et al. 2018 *Mater. Perform. Charact.* **7**/1 224-58
[5] Pearson M R et al. 2012 *J. Phys. Conf. Ser.* **382** 012025
[6] Bashir M et al. 2018 *IOP Conf. Ser. Mater. Sci.* **290** 012054
[7] ODIN COST Action 18203 (Brussels, BE: COST - EU) odin-cost.com
[8] Priya Sh, Inman D J (eds.) 2009 *Energy Harvesting Technologies* (New York, NY, USA: Springer)
[9] Kaźmierski T J (ed.) 2011 *Energy Harvesting Systems: Principles Modeling and Applications* (New York, NY, USA: Springer)
[10] Gljušćić P, Zelenika S et al. 2019 *Sensors* **19**/22 4922
[11] Gljuscic P et al. 2021 *Proc. 21st EUSPEN Int. Conf.* 131-4
[12] Ahmad M M et al. 2021 *Int. J. Energy Res.* **45**/11 15609-45
[12] Cai M, Yang Z, Cao J, Liao W 2020 *Energy Technol.* **8** 2000533
[14] Fu H et al. 2021 *Joule* **5**/5 1074-118
[15] Fu X, Liao W-H 2019 *J. Vib. Acoust.* **141** 031002
[16] Kathpalia B et al. 2018 *Smart Mater. Struct.* **27** 015024
[17] Marković E 2021 *M.Sc. Thesis* (Rijeka, HR: University of Rijeka)
[18] Perčić M, Zelenika S et al. 2020 *Friction* **8**/3 577-93
[19] University of Rijeka, Croatia, Precision Engineering Laboratory precenglab.riteh.uniri.hr/category/lab-equipment
[20] Dey A, Yodo N 2019 *J. Manuf. Mater. Process.* **3** 64
[21] Hernandez R et al. 2016 *Proc. 26th Ann. Int. Solid Freeform Fab. Symp. An Add. Manuf. Conf.* 939-50
[22] FlashForge Creator 3 www.flashforge.com/product-detail/1
[23] Mathews P G 2005 *Design of Experiments with MINITAB* (Milwaukee, WI, USA: ASQ Quality Press)
[24] Dean A et al. (eds.) 2015 *Handbook of Design and Analysis of Experiments* (Boca Raton, FL, USA: CRC Press)
[25] Hastie T et al. 2009 *The Elements of Statistical Learning* - 2nd ed. (New York, NY, USA: Springer)
[26] Draper N R, Smith H 1998 *Applied Regression Analysis* - 3rd ed. (New York, NY, USA: John Wiley & Sons)
[27] MS Excel Solver algorithms www.solver.com/excel-solver-algorithms-and-methods-used